Numerical simulation of cone penetration tests incorporating drainage effects

B. Dalnayak[1], S. Chatterjee[2]
Indian Institution of Technology Bombay, Mumbai, India
[1]23d0278@iitb.ac.in ,[2]sc@civil.iitb.ac.in

V. Singh[3], C. O'Loughlin[4]
Centre for Offshore Foundation Systems, The University of Western Australia, Perth, Australia
[3]vikram.singh@uwa.edu.au , [4]conleth.oloughlin@uwa.edu.au

H. Zhou[5]
Norwegian Geotechnical Institute, Perth, Australia
[5]hongjie.zhou@ngi.no

ABSTRACT: This paper presents results from numerical modelling of cone penetration tests (CPTs) incorporating drainage effects and compares these results with equivalent model scale CPTs conducted in a centrifuge. A coupled large deformation finite element modelling technique, implemented in the commercial software Abaqus/Explicit using the arbitrary Lagrangian-Eulerian method is presented. The study combines the hypoplastic sand model with hydro-mechanical coupling, which enables modelling of the CPT response of both loose and dense sand under a range of drainage conditions. This modelling technique was validated by comparing the numerical results with the drained cone tip resistance profile measured in the CPTs conducted in a centrifuge. Further simulations were carried out for partially drained and undrained conditions to evaluate the effect of the drainage conditions on cone tip resistance in both loose and dense sand. CPT tip resistance profiles and excess pore water pressure distributions were investigated for these analyses. The findings from this study contribute to numerical modelling and interpretation of CPTs performed under partially drained conditions.

1 INTRODUCTION

Cone penetration tests (CPTs) are widely used to characterise in-situ and laboratory soil beds. Although it is generally appropriate to assume drained and undrained conditions respectively for CPTs in sand and clay, partially drained responses are expected in intermediate soils, such as a silty sand. In reality, sand can also exhibit partially drained and undrained behaviour under fast loading conditions with relatively long drainage paths, such as those relevant to large diameter foundations under storm loading, where the sand response during individual load cycles may be partially drained (Jostad et al. 2022). Drainage conditions for penetration problems are often intepreted using the non-dimensional penetration velocity, $V = vd/c_v$, proposed by Finnie and Randolph (1994), where v is the penetration velocity, d is a characteristic dimension and c_v is the coefficient of consolidation. The penetration process is generally considered to be drained when $V < 0.01$ and undrained when $V > 30$ (Randolph 2004).

Cone penetration simulation involves moving boundaries and large deformations, which leads to mesh distortion. Severe distortion of the finite element mesh causes convergence problems and inaccuracies that eventually causes the simulation to fail. To overcome this issue, specialised large deformation finite element (LDFE) modelling techniques such as Coupled Eulerian-Lagrangian (CEL), arbitrary Lagrangian-Eulerian (ALE) are required (Wang et al. 2015). Although several drained cone penetration simulations using LDFE are reported in the literature (Pucker et al. 2013; Kouretzis et al. 2014; Fan et al. 2018, 2021; Chen et al. 2020; Su et al. 2022; Esfeh et al. 2025), finite element (FE) modelling approaches for partially drained CPTs are complex, computationally demanding, and limited because widely used FE tools do not natively support LDFE analysis and hydro-mechanical coupling simultaneously. To address this, Chatterjee et al. (2013), Ullah et al. (2018), Zhang et al. (2024) among others employed the "remeshing and interpolation technique using small strain"

(RITSS; Hu and Randolph 1998a, 1998b) method to perform LDFE analyses incorporating consolidation effects.

Hamann et al. (2015) proposed a workaround to implement hydro-mechanical coupling by exploiting the thermo-mechanical analysis feature in Abaqus/Explicit with CEL to simulate partially drained CPTs. This approach was further employed by Staubach et al. (2020, 2021) to model cyclic pile behaviour and to back analyse vibratory pile driving in saturated soil. A key advantage of using the inbuilt Abaqus solver for pore pressure calculation is that it is significantly more computationally efficient than using user-defined subroutines. Furthermore, the native techniques provide robust handling of mesh distortion related challenges and evolving geometries under large deformations without the need for additional user-defined code or extensive debugging.

This study adapts the workaround proposed by Hamann et al. (2015) with the computationally efficient ALE LDFE technique to numerically back analyse results from model scale CPTs conducted in a centrifuge and reported by Chow et al. (2018). The simulations use the hypoplastic sand model (Niemunis and Herle, 1997), and consider both loose and dense sand, and a range of drainage conditions from fully drained to undrained. The investigation examines how cone tip resistance, q_c, varies with drainage condition, excess pore pressure development in loose and dense sands, and the depth-dependent relationship between drained tip resistance, $q_{c,dr}$, and undrained tip resistance, $q_{c,un}$. The study provides a basis for improving the analysis of partially drained cone penetration tests using LDFE modelling.

2 DESCRIPTION OF NUMERICAL MODEL AND METHODOLOGY

2.1 Problem definition and numerical modelling approach

The model scale CPTs reported by Chow et al. (2018) were modelled using Abaqus/Explicit v6.14 (Dassault Systèmes). The experiments were performed at 50g using a cone diameter, d_c = 10 mm with a tip angle of 60°, at two relative densities, D_R = 31% and 83%. An axisymmetric numerical model was developed for the equivalent field scale cone, for which d_c = 0.5 m. The mesh configuration, geometry, and boundary conditions of the numerical model are shown in Figure 1. The numerical model has a domain size of $30d_c \times 30d_c$. A region of width $2.5d_c$ from the axisymmetric axis was selected as the ALE region where remeshing was applied. The FE mesh contains 21,853 CAX4RT elements, which are four noded reduced integration coupled temperature-displacement elements. The selection of coupled temperature-displacement elements for hydro-mechanical coupling is explained in Section 2.2. A structured mesh with element size of $d_c/20$ was generated in the ALE region. The ALE region was remeshed following Fan et al. (2018), with a 'frequency' of one (i.e., it was remeshed every calculation time increment) and a 'sweep' of three (i.e., the mesh was updated through three adjacent element layers). The 'improve aspect ratio' remeshing algorithm and 'volume smoothing' algorithm were used following the recommendation of Tolooiyan and Gavin (2011). By default, ALE tends to reduce mesh refinement in curved regions, increasing element size around the cone tip at deeper penetration stages. To counteract this effect, a curvature refinement factor, $\alpha_c = 2$ was used, as recommended by Jarast and Ghayoomi (2017).

The cone-soil interaction was modelled with a surface-to-surface contact formulation with pure master-slave relation. The contacting cone surface was assigned as the master surface, while the soil surface was defined as the slave surface. A frictional contact was applied at the cone tip with a friction coefficient of $\mu = 0.5\tan\phi_c$, where ϕ_c is the critical state friction angle. The shaft of the cone was assumed to be frictionless to allow isolation of the tip resistance. Additionally, the 'zipper technique' (Grabe and König 2004) was employed to accommodate soil movement along the axisymmetric axis.

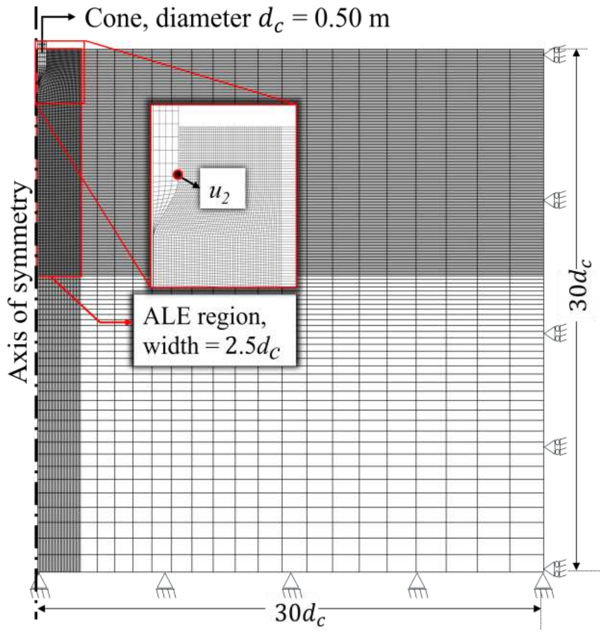

Figure 1. Numerical model showing FE mesh, boundary conditions and model geometry.

Sand behaviour was described using a hypoplastic sand model. The comprehensive hypoplastic model by von Wolffersdorff (1996), which was further improved by Niemunis and Herle (1997) introducing inter-granular strain, was adopted in this study. The model was implemented in the Abaqus/Explicit software using the VUMAT subroutine (Gudehus et al. 2008, Bienen et al. 2014). The hypoplastic parameters of the silica sand used in the experiments (Pucker et al. 2013) are given in Table 1.

Table 1. Hypoplastic parameters for the silica sand used in the Chow et al. (2018) experiments (Pucker et al. 2013).

Parameter	Value
ϕ_c [°]	31
h_s [MPa]	1354
n	0.34
e_{d0}	0.49
e_{c0}	0.76
e_{i0}	0.86
α	0.18
β	1.27
R	10^{-4}
m_R	5.16
m_T	3.07
β_R	0.58
χ	5.74

Results from the approach adopted in this study – in which the CPTs are simulated in a sand bed with vertically increasing stress, consistent with the experimental conditions – are compared with results from Singh et al. (2025), in which a uniform vertical stress at a depth of 2.5 m was assumed for both loose and dense sand. This comparison provided a basis for verifying the hydro-mechanically coupled LDFE analysis approach adopted here, as discussed later in Section 3.2.

2.2 Hydro-mechanical coupling technique

A hydro-mechanically coupled formulation is required to simulate cone penetration in saturated soil. The FE code Abaqus/Explicit does not (natively) support coupled pore fluid diffusion and stress analysis. Hamman et al. (2015) addressed this limitation by using the thermo-mechanical coupling capability within CEL to simulate partially drained pile driving within CEL in Abaqus/Explicit. This was achieved by drawing a term-by-term analogy between the governing equations of heat balance in thermo-mechanical analysis and mass balance of pore fluid in hydro-mechanical analysis such that the temperature represents the excess pore pressure. Staubach (2024) further refined this approach by incorporating frictional forces based on effective contact stresses. This study adapts this coupling approach into the ALE-based LDFE framework to simulate the centrifuge CPTs of Chow et al. (2018) across a range of drainage conditions, characterised by V. Following Staubach et al. (2020), a reduced value of bulk modulus of water, K_w = 5000 kPa, was considered which corresponds approximately to a degree of saturation of 95%. This simplification was deliberately chosen to optimise the computational time for the numerical simulations.

The penetration velocity was maintained at 10 mm/s for all cases. Different drainage conditions were simulated by varying the hydraulic conductivity (k) of soil, which altered c_v and in turn, V. This approach was adopted to avoid numerical instabilities of cone penetration at different penetration rates in ALE based CPT simulations as discussed by Fan et al. (2018) and Dalnayak et al. (2025). Figure 2 compares the q_c profiles for three penetration velocities: v = 10, 20 and 50 mm/s, with permeability, k (and hence c_v), adjusted for each penetration velocity such that V = 1 for each case. The coefficient of volume compressibility was taken as m_v = 0.00035 m^2/kN for both loose and dense sand. This corresponds to an effective vertical stress level of σ'_v = 20 kPa (Chow et al. 2018), which is approximately the vertical effective stress level at the mid-depth considered in the CPT simulations (z = 2.5 m). Depth profiles of cone tip resistance, q_c, on Figure 2 are essentially identical, indicating that maintaining a constant non-dimensional penetration velocity, V, in place of actual penetration velocity, v, can also effectively capture the intended drainage behavior.

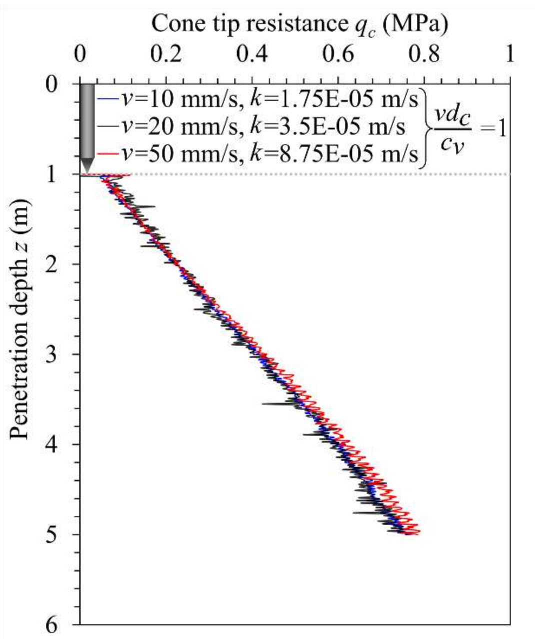

Figure 2. Comparison of q_c profiles at V = 1 in loose sand using different combinations of k and v.

3 RESULTS AND DISCUSSION

3.1 Comparison with the centrifuge CPT results of Chow et al. (2018)

Figure 3 presents q_c profiles for loose (D_R = 31%) and dense (D_R = 83%) sands for both drained conditions, and also for V = 1, 10 and 100 conditions. The experimental drained q_c profiles reported by Chow et al. (2018) for D_R = 31% and 83% are also included for comparison.

For the loose sand (D_R = 31%, Figure 3a), the drained cone tip resistance at the maximum penetration depth, z = 5 m, is $q_{c,dr}$ = 1.7 MPa which is only 6.6% lower than the measured value, $q_{c,dr}$ = 1.82 MPa. The agreement for the case of dense sand (D_R = 83%, Figure 3b) is good up to z = 3 m, but becomes poorer at greater depths with a numerically determined cone tip resistance at the maximum depth, z = 5 m of $q_{c,dr}$ = 5.96 MPa relative to the measured $q_{c,dr}$ = 8.25 MPa. This suggests that the hypoplastic parameters adopted from Pucker et al. (2013) are not well calibrated for dense sand over the range of stress levels in the Chow et al. (2018) experiments. Pucker et al. (2013) considered only one drained triaxial test at a mean effective stress of 80 kPa for calibration of the hypoplastic sand parameters. Fan et al. (2021) noted that the hypoplastic parameters proposed by Pucker et al. (2013) for this sand resulted in oedometer simulations at a relative density, D_R = 75%, that were in poor agreement with the experimental data in Pucker et al (2013) over vertical stresses up to 1 MPa.

CPT simulations for the loose sand on Figure 3a indicate that undrained conditions were reached at V = 100, as q_c at V = 100 is only marginally lower than at V = 10 – e.g., at a depth, z = 5 m, q_c = 0.79 MPa for V = 10, reducing by only 6% to q_c = 0.74 MPa at V = 100. This is consistent with other studies that generally considered undrained conditions to develop in the range V = 10 to 30 (e.g., see Randolph 2004).

The ratio of undrained to drained cone tip resistance from the CPT simulations for the loose sand is $q_{c,un}/q_{c,dr}$ = 0.74/1.7 = 0.44, which is close to the corresponding ratio from the measurements, $q_{c,un}/q_{c,dr} \approx$ 0.5. Numerical results for the intermediate non-dimensional penetration velocity, V = 1, gave q_c = 1.27 MPa at the final penetration depth, z = 5 m.

For the dense sand, the numerical simulations conducted for V = 10 and 100 are both considered to be undrained as both simulations produced essentially the same q_c depth profile. Numerically determined undrained cone resistance is around $q_{c,un}$ = 11.5 MPa after z = 5 m, about twice the measured value at the same depth. However, as discussed in the following paragraph, the agreement between the simulations and the measurements improves when the results are expressed as the ratio of the undrained to drained cone tip resistance.

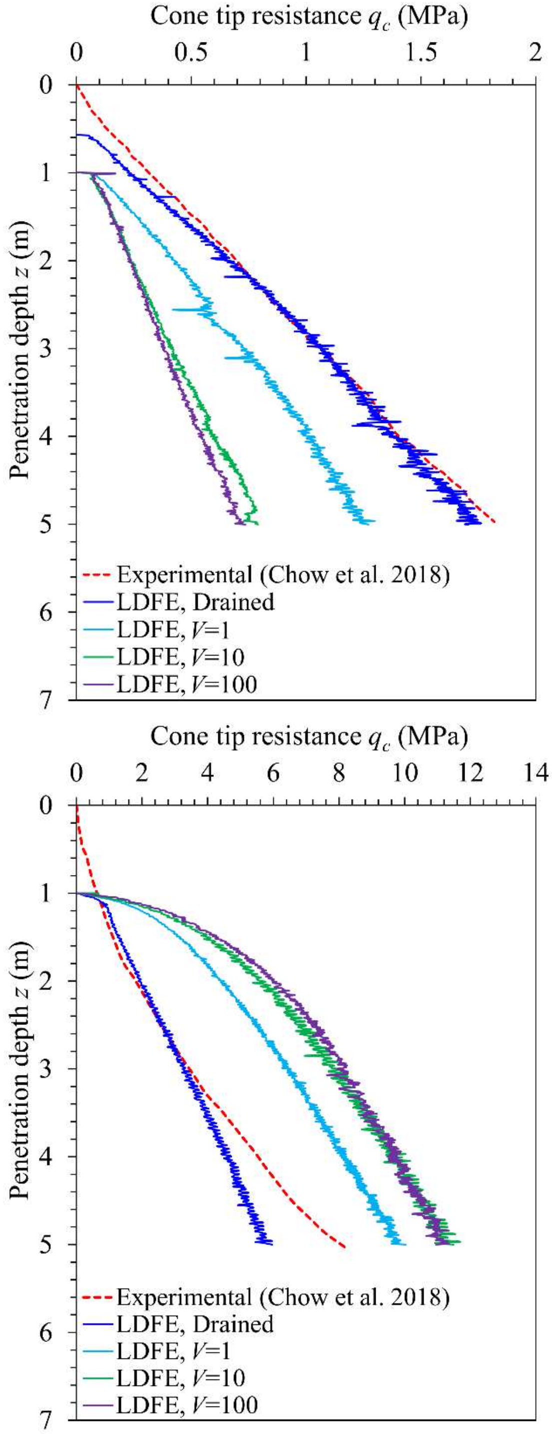

Figure 3. q_c profiles at different normalised velocities for: (a) loose (D_R = 31%) and (b) dense (D_R = 83%) sand.

Figure 4 shows how $q_c/q_{c,dr}$ varies with non-dimensional velocity, V, at different penetration depths. For the loose sand with D_R = 31%, $q_c/q_{c,dr}$ is approximately constant across the considered depths, with the steady state ratio of the undrained to drained cone tip resistance varying only slightly from $q_{c,un}/q_{c,dr}$ = 0.36 at z = 2 m (z = 4d_c) to $q_{c,un}/q_{c,dr}$ = 0.44 at z = 5 m (z/d_c = 10). Consequently, the drainage backbone curves for loose sand on Figure 4 are almost identical for the different depths.

For the dense sand with D_R = 83%, $q_{c,un}/q_{c,dr}$ varies between a maximum value of 3.27 at a depth, z = 1.6 m (z/d_c = 3.2) and 1.9 at z = 5 m (z/d_c = 10). The maximum value from the simulations, $q_{c,un}/q_{c,dr}$ = 3.27 is lower than the equivalent measured ratio, $q_{c,un}/q_{c,dr}$ = 4.95 reported by Chow et al. (2018), which was at a slightly shallower depth, z = 1.25 m. The range of $q_{c,un}/q_{c,dr}$ from the simulations decreases with increasing penetration depth and is in the range $q_{c,un}/q_{c,dr}$ = 1.9 to 3.27, compared to the experimantal range, which is approximately $q_{c,un}/q_{c,dr}$ = 0.7 to 4.95. These differences are not understood and are the subject of ongoing work.

Steady state cone penetration conditions are expected when the cone is sufficiently deep. There is evidence of this on Figure 4 when cone penetration increases to around z = 4 m, such that the backbone curves for z = 4 and 5 m are almost identical. At z = 5 m, $q_{c,un}/q_{c,dr}$ = 1.9, reducing to a steady state $q_{c,un}/q_{c,dr}$ = 1.8 at z/d_c = 14, lower than the steady state depth, z_{ss} = 17.5d_c calculated (for D_R = 83%) using the expression $(z/d_c)_{ss} \approx 2.2\exp(2.5D_R)$ proposed by Lehane et al. (2023) for silica sand.

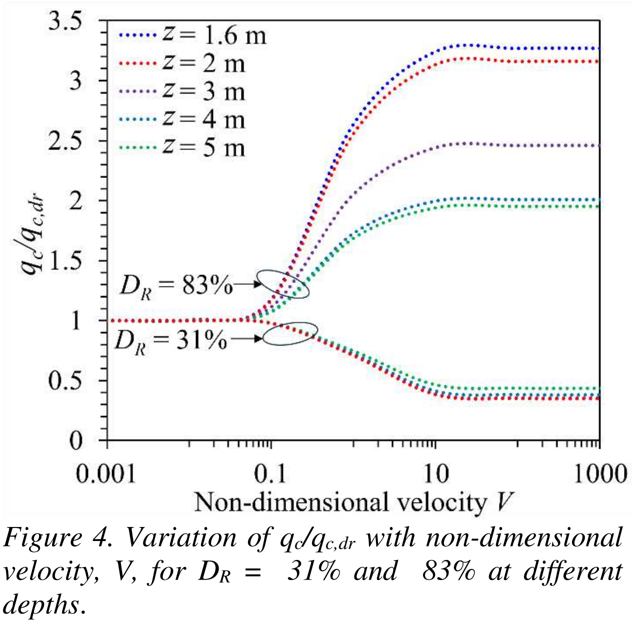

Figure 4. Variation of $q_c/q_{c,dr}$ with non-dimensional velocity, V, for D_R = 31% and 83% at different depths.

The numerically determined excess pore pressure field is presented in Figure 5 for V = 100 and for a penetration depth, z = 5 m. After a penetration, z = 4.6 m, the numerical simulation gives an excess pore pressure, Δp_w = 34 kPa for the loose sand at the u_2 location (cone shoulder – see Figure 1) for the undrained case, which compares favourably with the measured Δp_w = 30 kPa for V = 74 at the same penetration depth. As expected for dense sand, Δp_w is negative in the vicinity of the cone, as shown in Figure 5(b). This occurs because dense sand exhibits a dilative shearing response. The negative Δp_w increases the effective stress and, in turn, the soil resistance. As a result, cone tip resistance, q_c, increases with V as the penetration process transitions from drained to undrained. This increase in cone tip resistance, q_c, however, is limited by the cavitation limit of the pore water. In the centrifuge experiments there was a 60 mm water table maintained above the sand bed (as also considered in the numerical model), equivalent to 30 kPa of additional hydrostatic pressure. At z = 5 m this allows for a maximum negative pore pressure, Δp_w = -180 kPa before cavitation. In the numerical simulation the maximum absolute excess pore pressure for V = 100 was Δp_w = -178 kPa, as shown in Figure 5(b).

Despite some differences between the simulations and the experimental measurements, the simulated cone responses broadly reflect the measured trends and the expected drainage dependence for both loose and dense sand.

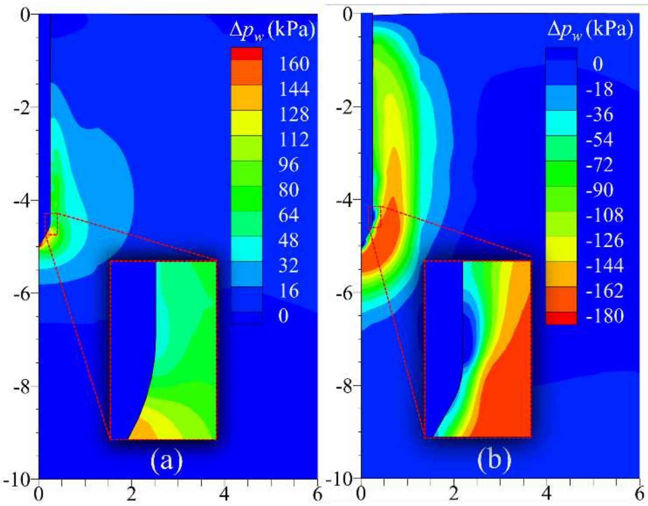

Figure 5. Excess pore pressure (Δp_w) contours at undrained penetration (V = 100) for: (a) loose sand (D_R = 31%) and (b) dense sand (D_R = 83%).

3.2 Comparison of partially drained cases with Abaqus/Standard

This section compares results from partially drained numerical CPTs from the present study with the CPT simulations of Singh et al. (2024), performed in Abaqus/Standard, where hydro-mechanical coupling is natively available. However, since Abaqus/Standard lacks remeshing capabilities, full

LDFE analyses cannot be conducted, and frictionless contact is typically used to delay mesh distortion and prevent numerical instabilities.

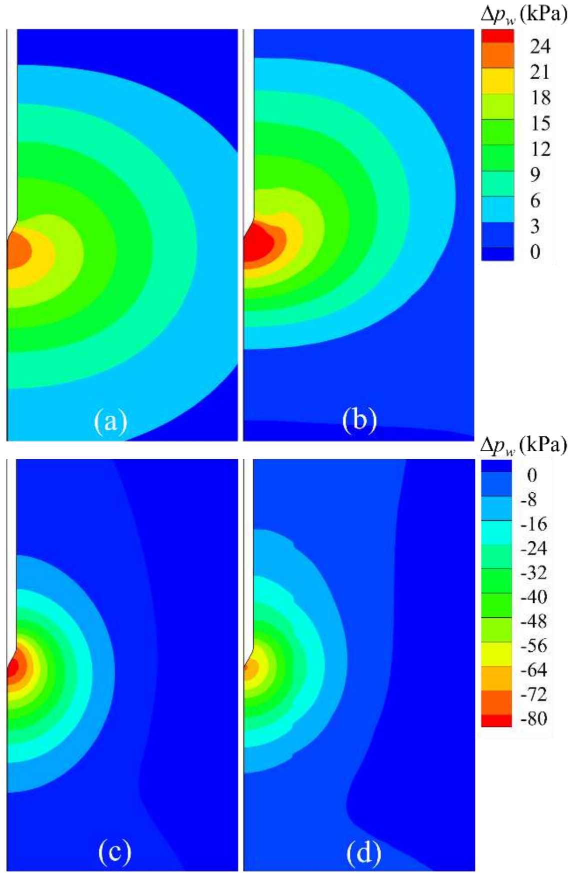

Figure 6. Excess pore pressure contours produced by Abaqus/Explicit and Abaqus/Standard at V = 1 for: (a) D_R = 31% (Abaqus/Standard), (b) D_R = 31% (Abaqus/Explicit), (c) D_R = 83% (Abaqus/Standard) and (d) D_R = 83% (Abaqus/Explicit).

Singh et al. (2024) modelled the CPT with a uniform vertical effective stress of $\sigma'_v = 23.9$ kPa for D_R = 31% and $\sigma'_v = 26.9$ kPa for D_R = 83% at $z = 2.5$ m. These conditions were replicated in the present study using the ALE-based LDFE approach in Abaqus/Explicit for both drained cases and for $V = 1$.

In Figures 6a and 6b, Δp_w distributions are compared for loose sand. The contours from both simulations are broadly consistent. Excess pore pressure near the cone tip reaches Δp_w = 29 kPa in Abaqus/Explicit, slightly higher than Δp_w = 24 kPa obtained using Abaqus/Standard. For dense sand, Δp_w distributions are compared in Figures 6c and 6d. The contours from both simulations are also consistent. Excess pore pressure near the cone tip reaches Δp_w = 79 kPa in Abaqus/Explicit, slightly lower than Δp_w = 85 kPa obtained using Abaqus/Standard. These minor differences in Δp_w are found to have minimal influence on the average cone response as reflected in the comparision of cone tip resistance using both methods shown in Figure 7. The q_c profiles obtained from both Abaqus/Explicit and Abaqus/Standard show

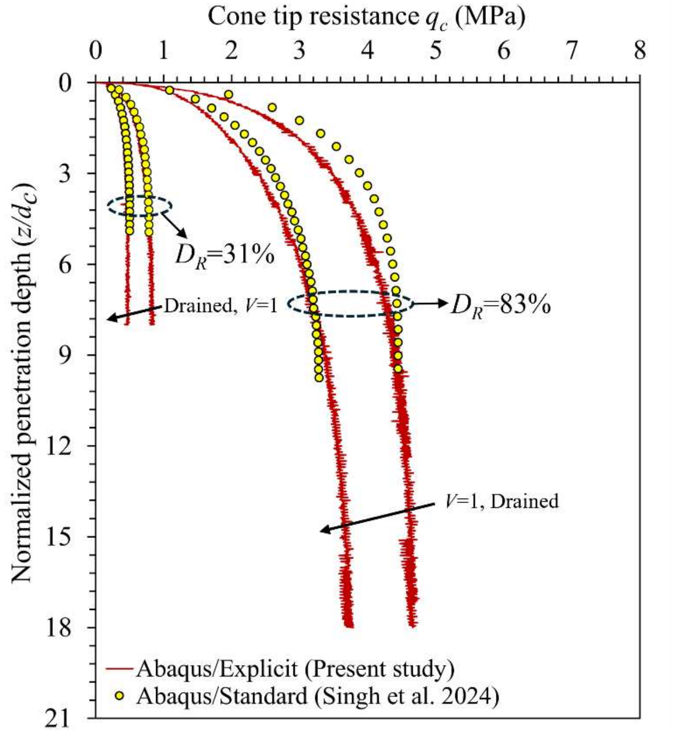

Figure 7. q_c profiles for drained and V = 1 obtained using Abaqus/Explicit and Abaqus/Standard.

good agreement. At $V = 1$, the cone tip resistance for the dense sand is $q_c = 4.53$ MPa in Abaqus/Explicit, slightly higher than $q_c = 4.45$ MPa obtained using Abaqus/Standard. For the loose sand at $V = 1$, Abaqus/Explicit gives $q_c = 0.49$ MPa, slightly lower than $q_c = 0.51$ MPa obtained using Abaqus/Standard.

4 CONCLUSIONS

This paper reports and discusses numerical simulations of model scale CPTs performed in a geotechnical centrifuge at different drainage conditions in both loose and dense sand. The numerical simulations employed the hypoplastic sand model and were implemented as ALE based hydro-mechanically coupled LDFE analyses in Abaqus/Explicit.

The simulations demonstrate the expected dependence of cone tip resistance on the drainage condition – as the response becomes progressively more undrained q_c increases in dense sand (due to shear-induced dilation) and reduces in loose sand (due to shear-induced contraction), consistent with the experimental observations. This variation in cone tip resistance from drained to undrained conditions is a reduction by about 56% for loose sand and an increase by about 180% for dense sand after reaching a steady state penetration depth. For the silica sand considered in the simulations, the cone response becomes undrained at a non-dimensional velocity, $V > 10$ for dense sand and $V > 100$ for loose sand. In loose sand the ratio of undrained to drained cone tip resistance achieves a steady value at cone penetration depths in excess of 4 cone diameters, whereas the equivalent depth in dense sand is 14 cone diameters. Results from the partially drained simulations were further validated through comparison with previously published results obtained using Abaqus/Standard.

In summary, the adopted thermo-mechanical analogy provides an effective approach for modelling effective stress behaviour in partially drained CPT simulations. The findings provide useful guidance for understanding expected cone responses in loose and dense sands and for numerically modelling partially drained CPTs using the ALE technique in Abaqus/Explicit.

ACKNOWLEDGEMENTS

This work was carried out as part of the collaborative research between the Indian Institute of Technology Bombay, the Centre for Offshore Foundation Systems (COFS) at the University of Western Australia, and the Norwegian Geotechnical Institute Perth. The third author is supported by the Australian Research Council Discovery Project grant (DP230101849) held by the fourth author.

REFERENCES

Bienen, B., S. Stanier, C. Vulpe, and D. Mašín., (2014). Interface enabling constitutive models coded as user materials to be employed in explicit analysis. GEO: 14756. Perth, Australia: Univ. of Western Australia, Centre for Offshore Foundation Systems.

Chatterjee, S., White, D. J., andand Randolph, M. F., (2013). Coupled consolidation analysis of pipe–soil interactions. Canadian Geotechnical Journal, 50(6), 609-619.

Chen, Z., Huang, M., and Shi, Z., (2020). Application of a state-dependent sand model in simulating the cone penetration tests. Computers and Geotechnics, 127, 103780.

Chow, S. H., Bienen, B., andand Randolph, M. F., (2018). Rapid penetration of piezocones in sand. In Cone penetration testing 2018 (pp. 213-219). CRC Press.

Chow, S. H., Roy, A., Herduin, M., Heins, E., King, L., Bienen, B., O'Loughlin, C., Gaudin, C., and Cassidy, M., (2019). Characterisation of UWA superfine silica sand.

Dalnayak, B., Singh, V., and Chatterjee, S. (2025). Numerical simulation of cone penetration in sand focusing on state parameter-based interpretation. GeoVadis: The Future of Geotechnical Engineering (Volume 1), 130.

Dassault Systèmes, 2014. Abaqus analysis 6.14 user's manual. Simulia Corp. Providence, RI, USA.

Fan, S., Bienen, B., and Randolph, M. F., (2018). Stability and efficiency studies in the numerical simulation of cone penetration in sand. Géotechnique Letters, 8(1), 13-18.

Fan, S., Bienen, B., and Randolph, M. F., (2021). Effects of monopile installation on subsequent lateral response in sand. I: Pile installation. Journal of Geotechnical and Geoenvironmental Engineering, 147(5), 04021021.

Finnie, I. M. S., and Randolph, M., (1994). Punch-through and liquefaction induced failure of shallow foundations on calcareous sediments. In Punch-through and liquefaction induced failure of shallow foundations on calcareous sediments (pp. 217-230). Pergamon.

Gamez, J. A., and Olson, S. M., (2022). Compressibility-based interpretation of cone penetrometer calibration chamber tests and corresponding boundary effects. Geotechnical Testing Journal, 45(4), 778-796.

Grabe, J. and König, F., (2004). Zur aushubbedingten Reduktion des Drucksondierwiderstandes. Bautechnik 81, No. 7, 569–577 (in German).

Gudehus, G., Amorosi, A., Gens, A., Herle, I., Kolymbas, D., Mašín, D., ... and Viggiani, G., (2008). The soilmodels.info project. International Journal for Numerical and Analytical Methods in Geomechanics, 32(12), 1571-1572.

Hamann, T., Qiu, G., and Grabe, J., (2015). Application of a Coupled Eulerian–Lagrangian approach on pile installation problems under partially drained conditions. Computers and Geotechnics, 63, 279-290.

Hu, Y., and Randolph, M. F., (1998a). A practical numerical approach for large deformation problems in soil. International Journal for Numerical and Analytical Methods in Geomechanics, 22(5), 327-350.

Hu, Y., and Randolph, M. F., (1998b). H-adaptive FE analysis of elasto-plastic non-homogeneous soil with large deformation. Computers and Geotechnics, 23(1-2), 61-83.

Jostad, H. P., Liu, H., Sivasithamparam, N., and Ragni, R., (2023). Cyclic capacity of monopiles in sand under Partially drained conditions: a numerical approach. Journal of Geotechnical and Geoenvironmental Engineering, 149(2), 04022129.

Jarast, P., and Ghayoomi, M., (2018). Numerical modeling of cone penetration test in unsaturated sand inside a calibration chamber. International Journal of Geomechanics, 18(2), 04017148.

Kazemi Esfeh, P., Senthen Amuthan, M., Bransby, M. F., Bienen, B., and O'Loughlin, C. D., (2024). Insights on cyclic cone penetration in sand from centrifuge and numerical modelling. Canadian Geotechnical Journal, 62, 1-16.

Kouretzis, G. P., Sheng, D., and Wang, D., (2014). Numerical simulation of cone penetration testing using a new critical state constitutive model for sand. Computers and Geotechnics, 56, 50-60.

Lehane, B. M., Zania, V., Chow, S. H., and Jensen, M., (2023). Interpretation of centrifuge CPT data in

normally consolidated silica and carbonate sands. Géotechnique, 73(10), 907-916.
Niemunis, A., and Herle, I., (1997). Hypoplastic model for cohesionless soils with elastic strain range. Mechanics of Cohesive-frictional Materials: An International Journal on Experiments, Modelling and Computation of Materials and Structures, 2(4), 279-299.
Pucker, T., Bienen, B., and Henke, S., (2013). CPT based prediction of foundation penetration in siliceous sand. Applied Ocean Research, 41, 9-18.
Randolph, M. (2004)., Characterisation of soft sediments for offshore applications. Proceedings of the 2nd International Conference on Site Characterization (Vol. 1, pp. 209-232). Porto, Portugal.
Singh, V., O'Loughlin, C., Zhou, H., and Bienen, B., (2024). Numerical Modelling of Cone Penetration in Sand Investigating Drainage Effects. In Indian Symposium on Offshore Geotechnics - An International Convention International Society for Soil Mechanics and Geotechnical Engineering.
Staubach, P., Machaček, J., Moscoso, M. C., and Wichtmann, T., (2020). Impact of the installation on the long-term cyclic behaviour of piles in sand: A numerical study. Soil Dynamics and Earthquake Engineering, 138, 106223.
Staubach, P., Machaček, J., Skowronek, J., and Wichtmann, T., (2021). Vibratory pile driving in water-saturated sand: Back-analysis of model tests using a hydro-mechanically coupled CEL method. Soils and Foundations, 61(1), 144-159.
Su, D., Wu, Z., Lei, G., and Zhu, M., (2022). Numerical study on the installation effect of a jacked pile in sands on the pile vertical bearing capacities. Computers and Geotechnics, 145, 104690.
Tolooiyan, A., and Gavin, K., (2011). Modelling the cone penetration test in sand using cavity expansion and arbitrary Lagrangian Eulerian finite element methods. Computers and Geotechnics, 38(4), 482-490.
Ullah, S. N., Hou, L. F., Satchithananthan, U., Chen, Z., and Gu, H., (2018). A 3D RITSS approach for total stress and coupled-flow large deformation problems using ABAQUS. Computers and Geotechnics, 99, 203-215.
von Wolffersdorff, P. A., (1996). A hypoplastic relation for granular materials with a predefined limit state surface. Mechanics of Cohesive-frictional Materials: An International Journal on Experiments, Modelling and Computation of Materials and Structures, 1(3), 251-271.
Wang, D., Bienen, B., Nazem, M., Tian, Y., Zheng, J., Pucker, T., and Randolph, M. F., (2015). Large deformation finite element analyses in geotechnical engineering. Computers and Geotechnics, 65, 104-114.
Zhang, Y., Fan, S., Li, S., and Shen, Z., (2024). Numerical analysis of the post-installation consolidated response of skirted foundations. Computers and Geotechnics, 166, 105931.